1174/90
v.2
c.1
Ref.

0 000 000 034039 J

INTERNATIONAL ATOMIC ENERGY AGENCY
UNITED NATIONS EDUCATIONAL, SCIENTIFIC AND CULTURAL ORGANIZATION
INTERNATIONAL CENTRE FOR THEORETICAL PHYSICS
I.C.T.P., P.O. BOX [illegible], 34100 TRIESTE, ITALY, CABLE CENTRATOM TRIESTE

H4.SMR/449-23

WINTER COLLEGE ON HIGH RESOLUTION SPECTROSCOPY

(8 January - 2 February 1990)

INTERNATIONAL CENTRE FOR THEORETICAL PHYSICS
21 JUN 1990
* LIBRARY *

LASER SPECTROSCOPY OF THREE-LEVEL SYSTEMS

E. Arimondo

Università di Pisa
Dipartimento di Fisica
Pisa 56100
Italy

LASER SPECTROSCOPY IN DOPPLER-BROADENED THREE-LEVEL SYSTEMS*

By E. Arimondo

Istituto di Fisica Sperimentale dell'Universita di Napoli**

(Received March 12, 1984)

In this paper the phenomena occurring in a three-level system inhomogeneously broadened by the Doppler velocity distribution and interacting with two monochromatic radiation fields are theoretically investigated in reference to different experiments. In the probe spectroscopy, where a radiation field is weak and does not perturb the populations differences and the level positions, a perturbation approach is convenient for determining the steady state density matrix elements. The probe response diagram has been introduced to derive the resonant conditions for the velocity groups participating to the processes. When both the radiation fields are strong and numerical solutions are required, the matrix continued fraction solution is convenient in the numerical analysis. The main features of the three-level phenomena are discussed and on the basis of typical parameters, the absorption lineshapes are analyzed.

PACS numbers: 32.70.Jz, 32.80.–t

1. Introduction

A large amount of spectroscopy and quantum optics experiments is based on three--level configurations, where two electromagnetic fields are quasi-resonant with two transitions sharing a common level. Making use of laser radiation, large modifications in the populations and in the level structure are introduced. They may be detected on the absorption or emission spectra of the connected transition. In experiments in dilute gas systems where the Doppler effect is the dominant process in determining the broadening of the absorption lines, monochromatic laser radiation selectively excites a velocity group within the velocity distribution and narrow sub-Doppler features appear on the observed spectrum. The three-level schemes are classified, depending on the level positions, in V, inverted-V and cascade configurations. Examples of experiments with the three-level systems occur in the two-photon spectroscopy, the double-resonance (with microwave or radio-

* Presented at the XI Summer School on Quantum Optics, Wieżyca, Poland, September 19–25, 1983.

** Address: Istituto di Fisica Sperimentale, Universita' di Napoli, Mostra d'Oltremare Pad. 20, 80125 Napoli, Italy.

frequency fields), the optically pumped lasers (in the optical and far-infrared regions), the optical-optical double resonance experiments, the mode-crossing and sideband spectroscopy, the non-linear Hanle effect and so on. For describing these different experiments specific models have been presented by several authors [1]. However a unified treatment of the three-level density matrix solution may allow one to interpret in a more complete and accurate manner the main features of the different experiments. Furthermore new phenomena may be predicted by transferring to some experimental configuration the results of a different configuration. Apart from the common features of the density matrix solution, the experiments are different in the values of the relaxation rates. The position of the resonances is affected very slightly by the values of the relaxation rates, but the lineshapes are greatly affected. Thus for each experiment the role played by the relaxation phenomena should be evaluated. In this paper we will analyze the resonances features of the steady state experiments on a theoretical basis, making use of different approaches and we will compare the numerical results to some specific experiments.

The experiments dealing with three-level systems may be classified as *probe-spectroscopy* or *strong-signal* ones, and such a division is relevant when a theoretical analysis is carried on. In the probe-spectroscopy a strong laser field, the so-called pump field, modifies populations and level structures, while the second field, the probe one, is weak and does not modify the populations and the level structure. A typical arrangement is the double-resonance experiments where the saturation phenomena produced by the pump radiation are monitored on a connected transition through the absorption (or emission) of a weak radiation field. The probe absorption may be increased by applying a stronger monitor field, but then the populations and the level structures modifications introduced by the probe laser should be considered. Thus in the strong-signal case the intensities of the pump and probe fields play a role in determining the position and the lineshape of the resonances. In the probe spectroscopy the probe field may be treated as a perturbation and the lowest order of the perturbation expansion is adequate to interpret the observed features. In the strong signal regime the higher orders of perturbation or an exact treatment are required.

The paper is organized as in the following: in Section 2 the main features of the three-level system will be presented. Section 3 will be devoted to the probe spectroscopy, with the general treatment, the "dressed" atom approach and some numerical analysis. Finally Section 4 will contain the treatment and the analysis of the strong-signal regime.

2. *The features of the three-level system*

2.1. Definitions

The three-level configurations may be analysed on the basis of a unified treatment. Figure 1 reports the possible configurations of this system with the common level 0 coupled to the 1 and 2 levels through the dipole materix elements $\vec{\mu}_{01}$ and $\vec{\mu}_{02}$ respectively. If the energy differences are denoted by $\hbar\omega_{ij}$ $(i, j = 0, 1, 2)$ and the quantities

$$\varepsilon_1 = \operatorname{sgn}(\omega_{01}), \quad \varepsilon_2 = \operatorname{sgn}(\omega_{02}) \tag{1}$$

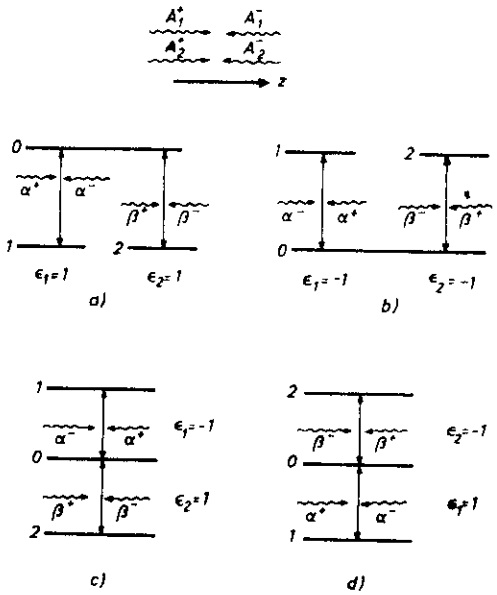

Fig. 1. Three-level system in different configurations. The definition of the Rabi flopping frequencies $\alpha^{\pm}$ and $\beta^{\pm}$ depending on the configuration following Eq. (3) is shown on the basis of the travelling wave $A_1^{\pm}$ and $A_2^{\pm}$ choice presented in the top of the figure

are introduced, each level configuration of Figure 1 is labelled by the $(\varepsilon_1 = \pm 1, \varepsilon_2 = \pm 1)$ indices. A phenomenon occurring in a configuration may be transferred to another one by changing the $(\varepsilon_1, \varepsilon_2)$ indices, and the configurations may be treated by a single formalism [2, 3].

The monochromatic pump and probe electromagnetic fields, $E_1(z, t)$ and $E_2(z, t)$ respectively, propagating along the z axis, will be described in a general configuration of travelling and standing waves through:

$$E_j(z, t) = \sum_{\mu = \pm 1} A_j^{\mu}[e_j \exp\{-i(\Omega_j t - \mu k_j z)] + \text{c.c.}]/2, \quad (j = 1, 2). \tag{2}$$

The index $\mu = \pm 1$ defines the counterpropagating components of the field. It will be supposed that owing to the frequency or polarization choice the E_1 field drives the $0 \rightarrow 1$ transition only and the E_2 field the $0 \rightarrow 2$ transition only. The coupling of the field with the three level system is described, within the rotating wave approximation, through the following Rabi flopping frequencies:

$$\alpha^{\mu} = (2\hbar)^{-1}\vec{\mu}_{01} \cdot (\vec{e}_1 A_1^{\mu}\delta_{\varepsilon_1,1} + \vec{e}_1^{*} A_1^{-\mu}\delta_{\varepsilon_1,-1}),$$
$$\beta^{\mu} = (2\hbar)^{-1}\vec{\mu}_{02} \cdot (\vec{e}_2 A_2^{\mu}\delta_{\varepsilon_2,1} + \vec{e}_2^{*} A_2^{-\mu}\delta_{\varepsilon_2,-1}). \tag{3}$$

Because of the introduction of the $(\varepsilon_1, \varepsilon_2)$ indices this definition is valid for any configuration of Fig. 1. [3].

The absorbers are submitted to the most general scheme of relaxation, including spontaneous decay and relaxation towards a set of external levels. The relaxation processes are taken into account by introducing some phenomenological damping constants as represented schematically in figure 2 for the V configuration. The total popula-

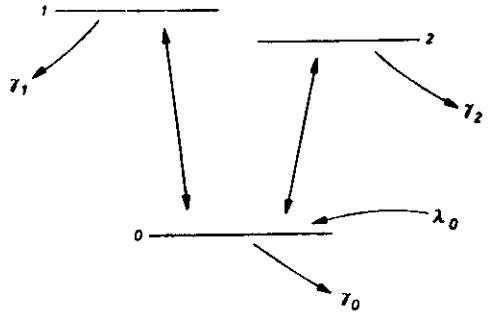

Fig. 2. Schematic representation of the V-configuration with the relaxation processes and the pumping mechanism λ_0 of the 0 level

tion relaxation rates, γ_j $(j = 0, 1, 2)$ are composed by the decay rates Γ_j to levels not included in the three-level system and the rate Γ_{ij} for the spontaneous decay or collisional population transfer from level j to level i. For the coherences, besides the relaxation processes introduced above, an additional rate γ_{ij}^c is introduced to describe the influence of laser instabilities and phase interrupting collisions. The role played by the velocity changing collisions in the probe spectroscopy has been analysed in a series of experimental and theoretical papers by Liao et al. [4]. These effects will not be considered in the present paper.

2.2. Travelling and standing waves

An important distinction in the analysis of the three-level phenomena has to be made between the case when both electric fields are in a travelling wave form, i.e. in Eqs. (2) the $\mu = 1$ or $\mu = -1$ term appears only, and when one or both electric fields are in a standing wave form. From the point of view of the phenomena a standing wave field produces several resonant structures in the absorption profile, whose resonant position is velocity dependent. Thus on the population distribution the saturation resonances (the so called Bennett holes) are produced within the Doppler distribution of the velocities. Furthermore velocity-dependent multiphoton resonances are produced by absorptions involving simultaneously the travelling photons of the standing wave. Finally the travelling wave electric fields give rise to Doppler-free structures where all the absorbers participated whichever is their velocity. In the V and inverted-V configurations of figures 1a and 1b, a Doppler-free Raman-type resonance appears for the co-propagating travelling waves when

$\varepsilon_1\Omega_1 - \varepsilon_2\Omega_2 = \omega_{21}$. In the cascade configuration of Figures 1c and 1d the Doppler-free resonances, the so called Doppler-free two-photon absorption, appears for counterpropagating travelling waves, but owing to the definition of the $(\varepsilon_1, \varepsilon_2)$ indices the resonant condition remains the same as written above.

From the theoretical point of view, the configuration with travelling wave components only, has, within the rotating wave approximation, an exact analytical solution for the density matrix equations. This rotating wave approximation, standard in the quantum optics treatment, does not include the Bloch-Siegert shifts that are negligible for the typical laser electric fields. The density matrix solutions have been presented by Brewer and Hahn [5] and by Takami [6] in a form convenient for numerical calculations. The role played by the relaxation rates and the radiation intensities in this scheme has been analysed in Refs. [7] and [8].

The standing wave configuration does not lead to an analytical solution of the density matrix equations in the Doppler broadened regime. In effect the steady state solutions of the v-velocity dependent ϱ_{ij} element for the density matrix should be written

$$\varrho_{ij}(v, z, t) = \exp\left[i(\varepsilon_i\Omega_i - \varepsilon_j\Omega_j)\right]\left\{\sum_{q_1=-\infty}^{+\infty} \varrho_{ij}^{q_1}(v)\exp\left(iq_1k_1z\right)\right.$$

$$\left. + \sum_{q_2=-\infty}^{+\infty} \varrho_{ij}^{q_2}(v)\exp\left(iq_2k_2z\right)\right\}, \quad (i, j = 0, 1, 2), \tag{4}$$

where we have introduced the $\varepsilon_0 = 0$ index.

This solution can be treated within a perturbation expansion in the radiation field intensities, as in Ref. [9]. Kyrola and Salomaa [10] have presented a different approximate solution for the density matrix in order to check the features of the three-level spectroscopy depending on the extension of the limits in the Doppler velocity integration. A straight numerical solution of the recurrence equations was applied by Paxton and Milonni in Ref. [11] to investigate the operation of two lasers operating in a three-level system. In Ref. [3] Vilaseca et al. have developed a matrix continued fraction solution valid for the standing wave problem and applied to investigate several experimental configurations.

2.3. Populations, coherences and level shifts

The striking feature of the three-level system is the creation of a coherence ϱ_{12} between the 1 and 2 states and its role in the absorption of radiation. Several experiments in quite different conditions have shown the influence of the ϱ_{12} coherence. In the V and inverted-V configurations of Figures 1a and 1b, if the 1 and 2 levels have nearly the same energy the relaxation rate of the ϱ_{12} coherence is small as compared to the relaxation rate of the optical coherences ϱ_{01} and ϱ_{02}. Thus large ϱ_{12} coherences are created with narrow resonant features. For instance in looking at the fuorescence from the 0 level in the inverted-V configuration, a narrow resonance dip appears when the two-quantum resonance condition of the $2 \rightarrow 1$ transition is satisfied. This phenomena called *coherence trapping* has been observed in several experiments, and the investigation of Gray et al. [12] has provided a detailed comparison between theory and experiment. Fig. 2, derived from the

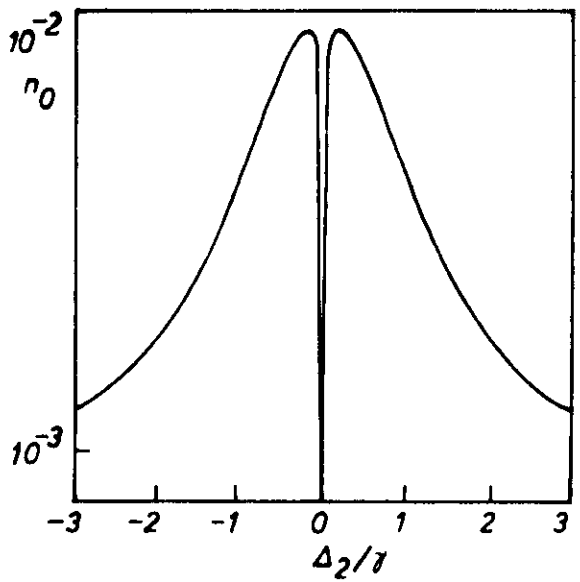

Fig. 3. Occupation of the 0 state in the inverted V-configuration as function of $\Delta_2 = \Omega_2 - \omega_{02}$, for irradiation at frequency Ω_2 and at frequency $\Omega_1 = \omega_{01}$, from Ref. [3]

theoretical analysis of Ref. [7], is a clear representation of the phenomenon. By keeping the Ω_1 frequency fixed to the resonant ω_{01} value and sweeping the Ω_2 frequency around the ω_{02} resonant value, the number of absorbers in the 0 state, and fluorescence from this state, presents a resonant increase. However at the center a narrow hole, a decrease in the resonance fluorescence, appears owing to the pumping of the absorbers into a $(|1\rangle - |2\rangle)/\sqrt{2}$ superposition, a non-absorbing state, where the absorption of the Ω_1 and Ω_2 photons does not occur. The full width of this hole is $(\alpha^2+\beta^2)/2(\gamma_{10}+\gamma_{12})$ in the low-field limit and the hole can be quite narrow, as shown in Fig. 3 and observed in the experiment of Gray et al. on a sodium atomic beam excited by two dye lasers.

Population phenomena are another important feature of the three-level system and the population pumpings produced by one radiation field give rise to interesting phenomena on the coupled transition. For instance Fig. 4 is an example, taken from Ref. [13], of the transferred Lamb dips observed on the output power of a far-infrared laser. In this experiment, based on the inverted-V configuration, the emission on the Ω_2 transition is observed while the pumping by strong radiation at the Ω_1 frequency in resonance with the ω_{10} transition provides the population in the upper level 0. For the optically pumped far-infrared lasers the pumping occurs through the CO_2 laser excitation in resonance with a roto-vibrational transition of the absorbing medium, and emission is produced on a rotational transition of the excited vibrational state. In a standing wave configuration for the pump field, Lamb dips are produced, i.e. the number of absorbers excited

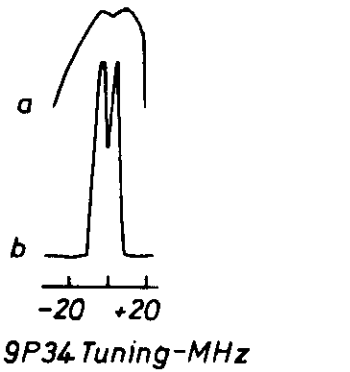

Fig. 4. Optoacoustic detection of the absorption in a FIR laser active medium in *a* and laser output power in *b*. An infrared Lamb dip is observed in the upper curve, and a transferred Lamb dip is detected in the laser emission

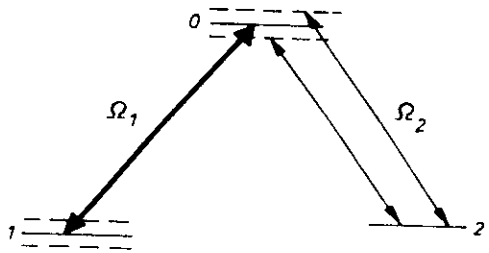

Fig. 5. Schematic representation of the Autler-Townes splitting when the $0 \rightarrow 1$ transition is excited by a strong Ω_1 field

to the upper 0 state decreases when the standing wave field is tuned at resonance $\Omega_1 = \omega_{10}$. This behaviour is demonstrated by the curve of Fig. 4a, where the absorption, detected through the optoacoustic effect, is recorded versus the laser frequency Ω_1. The decrease in the number of excited absorbers produces a decrease in the emitted power, as shown in the record of Fig. 4b. This population phenomenon is very useful in deriving molecular spectroscopy information from the optically pumped far-infrared operation and in using these lasers as very stable sources for frequency measurements [13].

The last important feature of the three-level system is the so called Autler-Townes effect or ac-dynamic Stark effect of the energy levels. The strong pump field produces a modification of the absorber behaviour, such that the absorption of the second radiation field presents, in the weak field limit, a double splitting of the resonant transition. The phenomenon is schematically represented in Fig. 5 where each of the 0 and 1 levels pumped by the Ω_1 field are splitted in two states, within the dressed atom approach, and the Ω_2

probe field has two resonant maxima for the transitions from the 2 level to the 0 level splitted states. In a Doppler-broadened medium the velocity dependent detuning produces a more complicated absorption splitting that will be analyzed in the following Section.

3. *Dressed-atom approach for probe spectroscopy*

The probe spectroscopy in presence of a strong standing-wave laser exhibits a rich variety of Doppler-broadened and Doppler-free structures, a sa consequence of the linear and non-linear interactions between the system and the waves involved. The standing-wave influences the probe response lineshape in two ways: a) modifying the velocity distibution of the level populations through the one- and multi-photon saturation resonances induced on the pump transition, i.e. the population effects, b) modifying the spectral response of each absorber according to its velocity through the multi-photon probe resonances and the ac-Stark effect, i.e. the nonlinear coherent effects. The multi-photon probe resonances are transitions involving few pump-photons and one probe-photon.

The saturation of a Doppler-broadened transition by a standing-wave pump with detuning $\Delta_1 = \Omega_1 - \omega_{01}$ produces Bennet holes in the population difference n_{01} of the velocities:

$$k_1 v = \pm \Delta_1/(2n+1) \tag{5}$$

owing to the $(2n+1)$-photon pump saturation resonances, as illustrated in Fig. 6 for the conditions of an experiment of probe spectroscopy that will be examined in the following. Shifts of the resonances may also occur because of non-resonant processes.

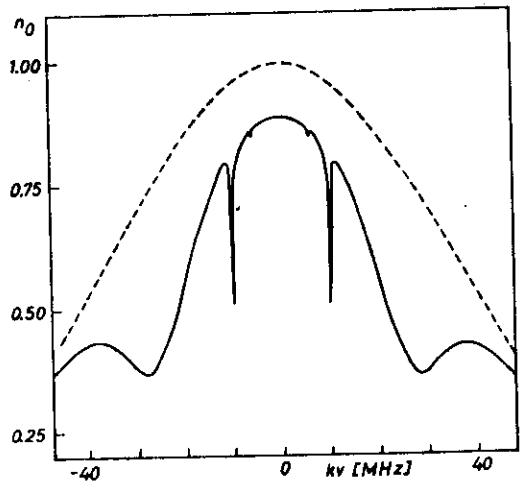

Fig. 6. Occupation of the 0 level versus the longitudinal Doppler shift kv for standing-wave irradiation on the $0 \rightarrow 1$ transition. The dashed line represents the population in absence of pump field. The parameters are $\alpha = 5$ MHz, $\gamma = 0.2$ MHz ($i = 0, 1, 2$), $ku = 50$ MHz, $\Delta_1 = 26$ MHz

The $W^{\pm}$ v-dependent absorption of the $\beta^{\pm}$ probe field may be expressed in terms of the field-free population differences as it follows [9]

$$W^{\pm}(v) = 2h\Omega_2|\beta^{\pm}|^2 \operatorname{Im}\{[n_{02}^0(v) + Tn_{01}^0(v)]/G\}, \tag{6}$$

where G and T depend on the flipping frequency $\alpha^+ = \alpha^- = \alpha$, the detunings $\Delta_j = \Omega_j - \omega_{0j}$, the Doppler shift $k_1 v$ and the relaxation rates. This dependence on the population goes through the $n_{02}^0 + Tn_{01}^0$ term, and the most general case is given by the linear combination of the cases $n_{01}^0 = 0$ and $n_{02}^0 = 0$. The term Tn_{01}^0 accounts for the population changes induced by the pump field. In experiments as in Ref. [14] where $n_{01}^0 = 0$, the pump population effects are not present. The nonlinear coherent effects are contained in $G(v)$ and their contribution to the absorption is weighted with the population difference.

The dressed-atom picture is a convenient approach to analyze the pump saturation effects and the probe resonances. This dressed-atom picture has been discussed by Berman and Salomaa in Ref. [15] within a comparison to the bare-atom picture, and more in detail by Roso et al. in Ref. [16]. In this last reference a probe response diagram has been introduced in order to determine the velocities and resonant processes that contribute to the velocity-averaged absorption as a function of the probe laser frequency, including the influence of the Doppler effect and of the ac dynamic Stark effect. Through the probe-response diagram the non linear coherent effects contained in the $G(v)$ term of Eq. (6) have been analyzed, in order to show the narrow structures in the velocity-averaged probe lineshape. Moreover the pump population phenomena contained in the Tn_{01}^0 term may be described through the dressed-atom approach.

In the atomic rest-frame, moving with v-velocity, the states $|1, n_+, n_-\rangle$ and $|0, m_+, m_-\rangle$ are introduced, where n_μ, m_μ with $\mu = \pm 1$ denote the photons of the travelling wave components of the pumping field at frequency $\Omega_1 + \mu k_1 v$. The above states are nearly degenerate if

$$n_+ + n_- + 1 = m_+ + m_- = N. \tag{7}$$

For a fixed total number of photons N there is an "infinite" ($\simeq 2 \times N$) number of states which must be diagonalized with coupling terms given by

$$\begin{aligned} \langle 0, n_+, n_-|H_1|1, n_+ + 1, n_-\rangle &= \alpha^+, \\ \langle 0, n_+, n_-|H_1|1, n_+, n_- + 1\rangle &= \alpha^-. \end{aligned} \tag{8}$$

Because of the choice of n_+ and n_- is unrelevant, a shortened label may be introduced

$$\begin{aligned} |0, n_+ - m, n_- + m\rangle &\equiv |0, q = 2m\rangle, \\ |1, n_+ - m, n_- + m + 1\rangle &\equiv |1, q = 2m+1\rangle, \end{aligned} \tag{9}$$

with energies of the uncoupled states calculated relatively to the $|0, 0\rangle$ state, given by

$$\begin{aligned} E_q^v &= \langle 0, q|H_0|0, q\rangle = q\bar{v}, \quad q \text{ even} \\ E_q^v &= \langle 1, q|H_0|1, q\rangle = \Delta_1 + q\bar{v}, \quad q \text{ odd} \end{aligned}$$

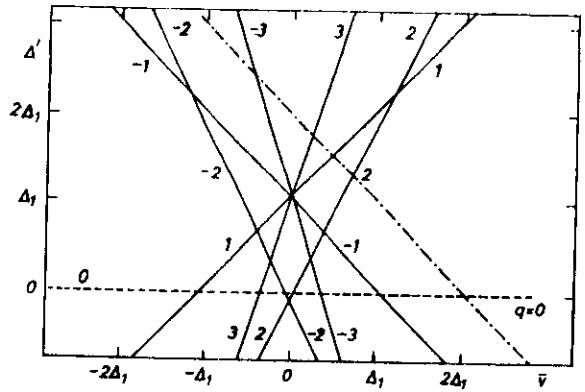

Fig. 7. Probe response diagram in coordinates $(\Delta', \bar{v})$ at $\Delta_1 \neq 0$, when the pump couplings are neglected. The broken line represents the probe energy given by Eq. (11)

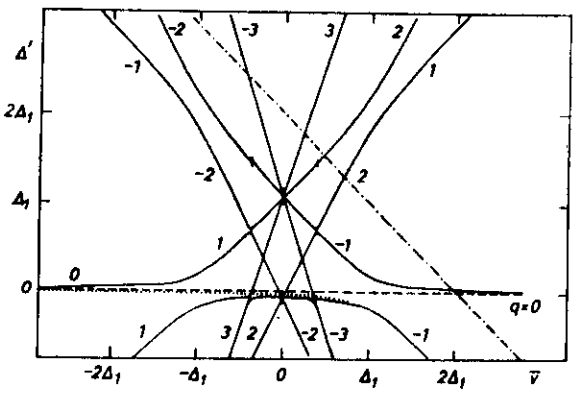

Fig. 8. Probe response diagram as in Fig. 7 including the couplings with the standing wave saturator ($\Delta_1 = 5.2\alpha$)

where $\bar{v} = k_1 v$ and H_0 is the Hamiltonian of the uncoupled atomic and photon states. An energy diagram may be constructed for the uncoupled and coupled states as reported in Figures 7 and 8 for the energy $\Delta' = \Delta_1 + q\bar{v}$ versus the reduced velocity $\bar{v}$ for a detuned saturator ($\Delta_1 \neq 0$). In Fig. 7 the even q lines cross at the (0, 0) coordinate points, and the odd q lines cross at the $(\Delta_1, 0)$ point. Owing to the interaction Hamiltonian of Eqs. (8) anticrossing points are created in the dressed atom energy level diagram of Fig. 8, as presented in Ref. [16]. The anticrossing points, resonant at velocities $\bar{v} = -\Delta_1/q$, $q = 1, 2, 3, \ldots$ produce the saturation resonances of Eqs. (5), i.e. the Tn_{01} term in the probe signal of Eq. (6). A coupling existing between the even q states of Eq. (8) does not modify the dressed energies, except for the case of the $v = 0$ stationary absorbers that must be treated differently [16].

The three-level probe spectroscopy is treated introducing the $|n_2\rangle$ photon states for the travelling wave probe at frequency Ω_2 and the $|2, n_+, n_-\rangle$ state of the absorber and the standing wave photons. Thus for the V-inverted configuration the manifold of the resonant unperturbed dressed states is composed by the following ones, with the shortened notations:

$$|0, n_+ - m, n_- + m, +n_2\rangle = |0, q = 2m, 0\rangle,$$

$$|1, n_+ - m, n_- + m + 1, n_2\rangle \equiv |1, q = 2m+1, 0\rangle,$$

$$|2, n_+, n_-, n_2 + 1\rangle \equiv |2, q = 0, 1\rangle. \tag{10}$$

The dressed energy diagram for the first two states is that represented in Fig. 7. The probe $|2, 0, 1\rangle$ state has unperturbed energy

$$E^u_{pr} = \langle 2, 0, 1|H_0|2, 0, 1\rangle = \Delta_2 - (k_2/k_1)\bar{v}, \tag{11}$$

represented by a broken line with slope $-k_2/k_1$ on the diagram of Fig. 7. The crossing of this probe line with the continuous line dressed energies define the resonant conditions for the multiphoton processes involving one probe photon:

$$\Delta_2 - k_2 v = q k_1 v \quad (q = 0, \pm 2, \ldots), \tag{12a}$$

$$\Delta_2 - k_2 v = \Delta_1 + q k_1 v \quad (q = 1, \pm 3, \ldots), \tag{12b}$$

where $|q|$ is the number of pump-photon involved in the process.

When the coupling of the standing-wave Hamiltonian is introduced in the dressed atom model, the diagram of Figure 8 results, with the broken line representing the probe state energy. The crossing of the probe line with dressed energies, as in Fig. 8, determines the resonant velocities for the multiphoton processes including the ac dynamic Stark effect, i.e. the influence of the pump field on the absorber energy levels. When the Ω_2 probe frequency is swept over the resonance frequency ω_{02}, the probe line is parallelly shifted along the horizontal axis and the resonant velocities are derived from the crossing points. The velocity integrated absorption signal is obtained summing up the contributions of the resonant velocities. Each velocity contribution is weighted by the transition rate $P_{|2,0,1\rangle \to |x_q\rangle}$ between the $|2, 0, 1\rangle$ probe level and the dressed level $|x_q\rangle$ and the population difference between the dressed levels.

The effects of populations created by an incoherent pumping and relaxation mechanism may be included into the dressed-atom picture, as shown in Refs. [17, 15] and thus the absorption profile derived. However the bare-atom picture is more convenient for quantitive comparisons.

The response of the stationary absorbers in the presence of a SW saturator is more readily derived by taking explicit account of the spatial-inhomogeneity of the field and the spatial distribution of the absorbers. In effect, in classical terms an absorber located at the z position experiences the standing wave pump as a monochromatic field of amplitude $2A_1 \sin k_1 z$ ($A_1^+ = A_1^- = A_1$). This interaction can be described by the travelling wave

solution, where a space dependent Rabi frequency

$$\Omega_R(z) = 4\alpha \sin k_1 z \tag{13}$$

is introduced. The dressed energies for the case of a travelling wave saturator describe the modifications introduced by the Autler-Townes or ac dynamic Stark effect represented in Fig. 5. For the stationary absorber at position z, if $\Delta_1 = 0$, the dressed energies may be written as follows

$$E_0(z) = \xi_{r=0},$$
$$E_1(z) = -\xi_{r=0}, \tag{14}$$

with

$$\xi_{r=0} = \Omega_R(z)/2 \tag{15}$$

being the spatially-inhomogeneous perturbation suffered by the stationary absorbers.

The levels of Eq. (14), represented as a function of z cover the -2α to 2α energy interval as a consequence of the spatially-inhomogeneous ac Stark shift $\xi_{r=0}$ (figure 8). The innermost ends of the interval are related to absorbers located at the nodes of the standing wave pump, where the shift vanishes, and the outermost ends to absorbers at the antinodes, where the shift is maximum. If a uniform spatial distribution of the absorbers is assumed, the density of dressed levels as a function of the energy is defined by $(\partial E_0/\partial z)^{-1}$ and $(\partial E_1/\partial z)^{-1}$. It shows maxima at the two extremities of both intervals because the shift $\xi_{r=0}$ changes more slowly with z around the antinodes than in other regions.

Fig. 9 shows the influence of the nonlinear coherent effect produced by a detuned standing wave saturator ($\Delta_1 = 5.2\alpha = 130\gamma$) on the spectral response of the probe laser,

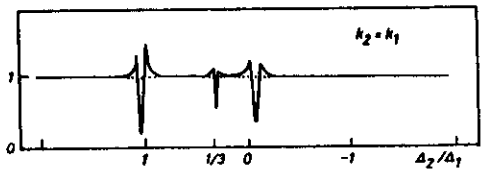

Fig. 9. Probe absorption spectra (in arbitrary units) showing the non-linear coherent effects produced by a well detuned standing-wave saturator, with $k_1 = k_2$, $k_1 u = 10^6\gamma$, $n^0_{10} = 0$ and $n^0_{20} = 1$

for the ratio $k_1/k_2 = 1$. Populations effects are absent because $n^0_{10} = 0$ was supposed. These spectra may be interpreted with the energy diagram of Fig. 8, which corresponds to the same Δ_1/α ratio. For the spectrum the probe level E^u_{pr}, with slope $-k_2/k_1$, must be swept on the diagram and the intersection with E_q levels examined. For Δ_2 values higher than Δ_1, E^u_{pr} intersects several E_q levels at different $\bar{v}$ velocities but the absorption is determined mainly by the E_0 level, which is almost unperturbed in this region. Hence this part of the spectrum due to the $q = 0$ single-photon process follows the Doppler background

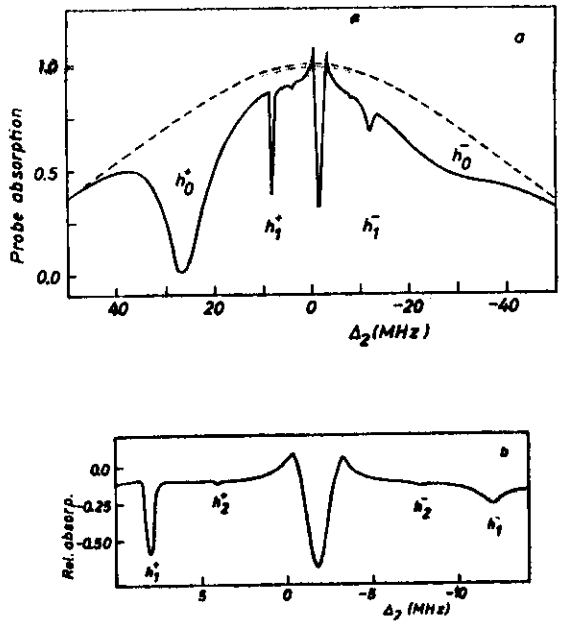

Fig. 10. At the top the normalized probe absorption cofficient versus the frequency detuning Δ_1 for the weak probe $\beta = 0.005$ MHz and the parameters of Fig. 6 corresponding to the experiment of Ref. [18]. In the bottom curve the central part of the probe absorption as obtained by an on-off modulation of the pump radiation is shown

of the population distribution. For Δ_2 values around Δ_1 the absorption results from the E_0 level through absorbers with $\bar{v} \sim \Delta_1$ and from the E_{-1} level, at which all the velocities contribute. The ac Stark effect modifies such contributions as a function of Δ_2 and originates the peculiar structure appearing in the $\Delta_2 \sim \Delta_1$ part of the spectrum. More precisely, a first peak occurs when E^u_{pr} coincides with E_{-1} in the low energy interval, a second peak when E^u_{pr} coincides with E_1 in the high-velocity intervals. Thus these peaks are due to the two-photon process. In between these peaks intersects at none velocity the E_0 and E_{-1} levels. Thus the absorption diminishes and a dip appears. The peak at $\Delta_2 = \Delta_1$, produced by the high-velocity absorbers, diminishes with decreasing the Doppler width and disappears for $k_2 u < 2\Delta_1$.

The structure near $\Delta_2 = \Delta_1/3$ appears when E^u_{pr} comes across the level anticrossing (0, 3) produced by the three-photon saturation resonance on absorbers with $\bar{v} \sim \Delta_1/3$. The lack of absorption at the anticrossing center originates a dip. The $\Delta_2 \sim 0$ structure is related to the spatially-inhomogeneous ac Stark shift suffered by the $v = 0$ absorbers. It appears when E^u_{pr} intersects the energy interval covered by $E_0(z)$. The lineshape is determined by the nonuniform distribution of absorbers along the energy interval. For $\Delta_2/\Delta_1 < 0$ values no structure appears, the remaining Doppler-broadened background being due to

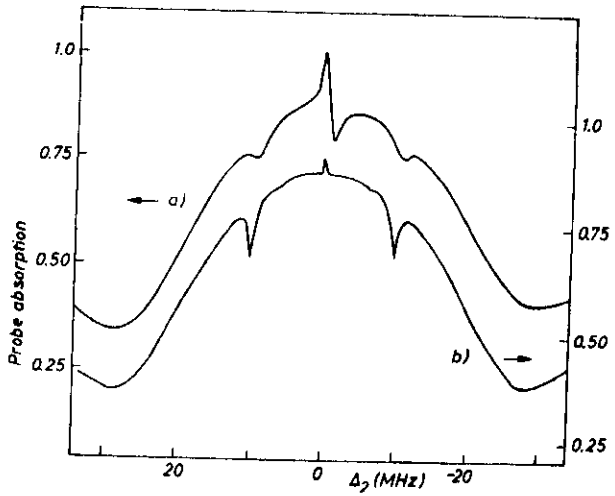

Fig. 11. The normalized probe absorption coefficient versus the frequency detuning Δ_2 in presence of a relaxation rate γ_{12}^c

the E_0 and E_1 levels. Let us remark that in spite of the very similar lineshape, the three main features of the spectrum have a completely different origin.

Fig. 10a represents the probe absorption resulting from the same parameters used in the previous figure except for the Doppler-width $k_1 u/\gamma = 100$ corresponding to an experiment on the three-level system in an infrared region, Ref. [18]. In this experiment Reid and Oka applied a modulation technique to eliminate the Doppler profile of the probe absorption, as it was done in Fig. 10b, supposing an on-off modulation of the pump field. Figure 10a and b are very similar to those reported in the above experiment. There the central feature appeared with a slightly different lineshape that may be ascribed to the presence of the m-degeneracy and a distortion introduced by the Stark modulation in the intracavity experiment. These probe absorption spectra were discussed in Ref. [19].

The coherent phenomena occurring at $\Delta_2 = 0$ are determined by the coherent interaction of the Ω_1 and Ω_2 waves on the system and depend on the existence of the two-quantum coherence ϱ_{12}. Thus if a relaxation mechanism is introduced to destroy specifically the ϱ_{12} coherence, these phenomena disappear. This is shown in Fig. 11 where the probe absorption is reported supposing $\gamma_{12}^c = 30$ and 300 MHz respectively. The stationary absorber signal is distorted or destroyed by the γ_{12}^c rate, because the radiative shift of the ac Stark effect involves the two-quantum ϱ_{12} coherences. At large γ_{12}^c the dispersion derivative signal disappears and a narrow symmetrical peak centered at $\Delta_2 = 0$ appears. This signal at the center of the probe absorption spectrum allows an absolute measurement of the transition frequency with a natural linewidth resolution even at large pump power [20].

4. Strong signal regime

When neither of electromagnetic fields acting on the three-level system is weak and the perturbation approach of the probe spectroscopy cannot be applied, a large amount of numerical computation is required to analyze the behaviour of the detected signal. Few experiments have been concerned with the strong signal regime. Some investigations [21, 22] have dealt with the velocity-tuned multiphoton transitions, where a strong electromagnetic field simultaneously excites the $1 \rightarrow 0$ and $0 \rightarrow 2$ transitions of the three-level system. For the lasers operating simultaneously on two transitions sharing a common level [23], for the optically pumped lasers in the visible [24] and far-infrared regions [25], a strong signal treatment is required. Such an analysis may be also required in the experiments of Refs [14, 18], if a strong probe laser would be used. From the theoretical point of view Paxton and Milonni [11] have solved numerically the recurrence relations satisfied by the density matrix elements in order to analyze the behaviour of a laser operating simultaneously on two coupled transitions. Vilaseca et al. [3] have shown that starting from the recurrence relations for the density matrix elements, the solution may be expressed through matrix continued fractions, a convenient approach for numerical analysis. In the most general case the solution involves matrices of infinite order. However without loss of generality it may be supposed that two integers a and b can be defined such that a/b is a rational number and for the k_1 and k_2 wavenumbers

$$k_1 = ak, \quad k_2 = bk, \tag{16}$$

where k is a reduced wavenumber. The steady statee solution for the density matrix elements may be written as

$$\varrho_{ij}(v, z, t) = \exp\left[i(\varepsilon_i\Omega_i - \varepsilon j\Omega_j)t\right] \sum_{q=-\infty}^{\infty} \varrho_{ij}^q(v) \exp(iqkz) \quad (i, j = 0, 1, 2). \tag{17}$$

Thus the solution involves vector and matrices of 4θ dimensions, θ being the largest one of the a and b numbers.

However we have found that several important configurations may be solved through a recurrence relation involving vectors and matrices with dimension 4. An important case is when the wavenumbers k_2 and k_1 are equal, or more precisely if $|k_1 - k_2|$ is smaller than the inverse of the Δz distance covered by the absorbers with velocity v during the interaction time with the electromagnetic fields. Another important case occurs when $k_2 = 0$, i.e. when the Doppler broadening of the $0 \rightarrow 2$ transition is negligible, as for a radiofrequency, microwave or long-wavelength far-infrared transition. If $k_2 = 0$ the two counterpropagating β^+ and β^- fields cannot be distinguished and this case is formally equivalent to thet of a travelling wave, the last case where the 4 dimension vectors and matrices apply.

In these cases the steady state equations of the density matrix elements may be written

$$W_q^{-1} X^{q-2} + W_q^0 X^q + W_q^1 X^{q+2} = I^0 \delta_{q,0} \tag{18}$$

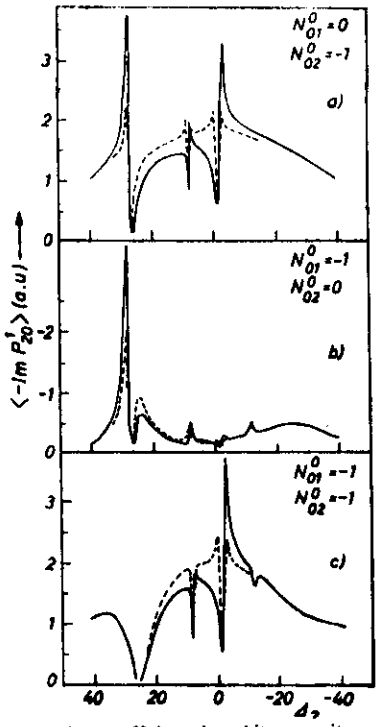

Fig. 12. Velocity-integrated absorption coefficient, in arbitrary units, versus the frequency detuning Δ_2 for various zero-field population differences. Parameters are given in the text

where

$$X^q \equiv \begin{bmatrix} \varrho_{00}^q - \varrho_{11}^q \\ \varrho_{00}^q - \varrho_{22}^q \\ \varrho_{12}^{q+a-b} \\ \varrho_{21}^{q-a+b} \end{bmatrix}, \qquad I^0 \equiv \begin{bmatrix} n_{01}^0 \\ n_{02}^0 \\ 0 \\ 0 \end{bmatrix}, \tag{19}$$

with $n_{0i}^0 (i = 1, 2)$ the pumping terms and the elements of the W_q^μ 4×4 matrices written in the appendix of Ref. [3]. The solution of the recurrence relations (18) may be formally written

$$X^0 \equiv \{W_0^{-1} Z_{-2}^{-1} + W_0^0 + W_0^1 Z_2^1\} I^0,$$
$$X^q \equiv Z_q^{\pm 1} X^{q \mp 2}. \tag{20}$$

and the matrix continued fractions Z_q^μ ($\mu = \pm 1$) are given by

$$Z_q^\mu = -(W_q^0 + W_q^\mu Z_{q+2\mu}^\mu)^{-1} W_q^{-\mu}. \tag{21}$$

The continued fractions (21) are evaluated numerically by truncation to a finite number of terms in the denominator. The analysis of probe spectroscopy with a weak travelling

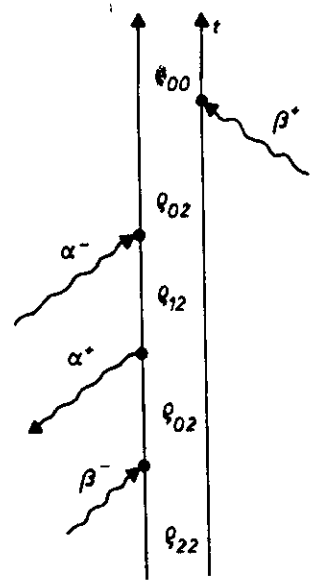

Fig. 13. A Feynman diagram of the density matrix for the pump-field Rayleigh-type processes considered in the text

wave (TW) when a strong slightly-detuned standing wave (SW) laser pumps a transition sharing a level with the probe transition was presented above. A comparison was made with the infrared laser intracavity experiment by Reid and Oka [18]. Referring to this experiment the modifications that would be introduced for the case of a SW probe may be analyzed. Thus the crosstalk terms appearing in the absorption spectrum by the presence of β^+ and β^- counterpropagating probe field are investigated. Unless otherwise stated the following parameters are used (all frequencies are expressed in units of true, not angular, frequencies):

$$\alpha^+ = \alpha^- = \alpha = 5 \text{ MHz}, \quad \Delta_1 = 26 \text{ MHz},$$
$$\beta^+ = \beta^- = \beta = 0.005 \text{ MHz}, \quad ku = 50 \text{ MHz},$$
$$\Gamma_0 = \Gamma_1 = \Gamma_2 = \Gamma = 0.2 \text{ MHz}, \quad \gamma_{ij}^c = \Gamma_{ij} = 0 \quad \forall_{i,j},$$

i.e. the SW pump couples to the $0 \rightarrow 1$ transition while the SW probe couples to the $0 \rightarrow 2$ transition. As typical of infrared molecular transitions, only collisional relaxation to states external to the three-level system is introduced for the level population. The cases where the population is initially concentrated in either state 1 or state 2 or in both states 1 and 2 are analyzed.

The velocity-integrated absorption of the β^- component of the SW probe versus the frequency detuning Δ_2 is plotted in Fig. 12 for the different zero-field population differences.

The dashed lines, shown for comparison, represent the β^+ absorption in the case of a TW probe (i.e. $\beta^- = 0$), all other parameters fixed to the values reported above. The results of Fig. 12c for both n_{01}^0 and $n_{02}^0 \neq 0$ are obtained summing up those of Figs. 12a and 12b.

Significative differences are produced in the β^+ absorption spectrum by the presence of the counterpropagating β^- field. The polarization induced by the simultaneous action of one β^+ photon and a pair of α^+, α^- photons (up-down α process) has a spatio-temporal dependence in phase with the β^- field and then influences its propagation. Fig. 13 shows a density matrix Feynman diagram describing a typical process involved in this $\beta^+ - \beta^-$ coupling. A Rayleigh scattering of α^+ and α^- photons is involved. The probability of these processes will resonantly increase whenever the intermediate level $|1\rangle$ approaches a level of the absorber "dressed" by the strong SW field.

5. *Conclusions*

It has been shown that in the Doppler-broadened three level spectroscopy several phenomena simultaneously contribute to the resonant features appearing in the absorption (or emission) spectra. For the probe spectroscopy, where a radiation field is weak, the physical processes determining the spectrum may be interpreted on the basis of the probe response diagram. The dressed system approach, with new features created by the velocity distribution, is a very convenient method for deriving the probe response diagram and allow one to obtain analytical expressions for the resonance conditions. The stationary absorbers constitute a special case because the lack of Doppler shift introduces an infinite degeneracy in the dressed system hamiltonian. In the strong signal regime where both electromagnetic fields are strong and perturbation approaches cannot be applied, the density matrix equations have to be solved exactly. By assuming that the wavenumbers of the electromagnetic fields are in the ratio of two a and b integer numbers, the solution of the density matrix equations can be expressed through continued fractions of dimensions four times the largest one between the a and b numbers. However several important cases of the three level spectroscopy may be solved through matrices of dimension four. That occurs (*i*) for $k_1 = k_2$, as in multimode crossings or sideband spectroscopy; (*ii*) when the Doppler shift of one transition is negligible, as in the double-resonance experiments with the laser pumping; (*iii*) for a travelling wave pumping combined with a standing wave oscillation or an adjacent transition, typical of some laser systems.

In each configuration the role played by the relaxation phenomena should be carefully evaluated, because it may modify considerably the spectrum lineshape. For instance the long relaxation rates for the coherence lead to the coherence trapping features, with narrow resonance lines. Moreover new narrow features, produced by the stationary absorbers at the center of the probe spectrum are predicted from the presented analysis in the probe spectroscopy. Finally other features produced by the relaxation phenomena are presented by the paper of Gawlik [26] at this school.

REFERENCES

[1] V. P. Chebotayev, in *Coherent Non-Linear Optics*, Eds. M. S. Feld and V. S. Letokhov, Springer-Verlag, Berlin 1980, p. 59–109.

[2] Th. Hansch, P. Toschek, *Z. Phys.* **236**, 213 (1970).

[3] R. Vilaseca, G. Orriols, L. Roso, R. Corbalan, E. Arimondo, *Appl. Phys.* **B34**, 71 (1984).

[4] P. F. Liao, J. E. Bjorkholm, P. R. Berman, *Phys. Rev.* **A20**, 1489 (1979); **A21**, 1927 (1980); P. R. Berman, P.F. Liao, J. E. Bjorkholm, *Phys. Rev.* **A20**, 2389 (1979).

[5] R. G. Brewer, E. L. Hahn, *Phys. Rev.* **A11**, 1641 (1975).

[6] M. Takami, *Jpn. J. Appl. Phys.* **15**, 1063, 1089 (1976).

[7] E. Arimondo, G. Orriols, *Lett. Nuovo Cimento* **17**, 333 (1976).

[8] A. Sasso, E. Arimondo, *Lett. Nuovo Cimento* **37**, 417 (1983).

[9] B. J. Feldman, M. S. Feld, *Phys. Rev.* **A5**, 899 (1972).

[10] E. Kyrola, R. Salomaa, *Phys. Rev.* **A23**, 1874 (1981).

[11] A. H. Paxton, P. W. Milonni, *Opt. Commun.* **34**, 111 (1980); *Phys. Rev.* **A26**, 1549 (1982).

[12] H. R. Gray, R. M. Whithey, C. R. Stroud Jr., *Opt. Lett.* **3**, 218 (1978).

[13] M. Inguscio, in *Advances in Laser Spectroscopy*, Eds. F. T. Arecchi, F. Strumia and H. Walther, Plenum Press 1983, p. 297–308.

[14] A. Schabert, R. Keil, P. E. Toschek, *Opt. Commun.* **13**, 265 (1975); R. Keil, P. Toschek, *Sov. J. Quantum Electron.* **8**, 949 (1978); J. Bialas, W. J. First, P. Toschek, *Opt. Commun.* **36**, 317 (1981); **37**, 451 (1981).

[15] P. R. Berman, R. Salomaa, *Phys. Rev.* **A25**, 2667 (1982).

[16] L. Roso, R. Corbalan, G. Orriols, R. Vilaseca, E. Arimondo, *Appl. Phys.* (Germany) **B31**, 115 (1983).

[17] C. Cohen-Tannoudji, S. Reynaud, *J. Phys. B* **10**, 345, 2311 (1977); S. Reynaud, Thesis, University of Paris 1981, unpublished.

[18] J. Reid, T. Oka, *Phys. Rev. Lett.* **38**, 67 (1977).

[19] R. Corbalan, G. Orriols, L. Roso, R. Vilaseca, E. Arimondo, *Opt. Commun.* **38**, 113 (1981).

[20] R. Corbalan, G. Orriols, L. Roso, R. Vilaseca, E. Arimondo, *Opt. Commun.* **40**, 29 (1981).

[21] J. P. Woerdman, M. F. H. Schuurmans, *Opt. Commun.* **21**, 243 (1971).

[22] M. Himbert, S. Reynaud, J. Dupont-Roc, C. Cohen-Tannoudji, *Opt. Commun.* **30**, 184 (1979).

[23] H. Schlemmer, D. Frolich, H. Welling, *Opt. Commun.* **32**, 141 (1980).

[24] B. Wellegehausen, H. H. Heitmann, *Appl. Phys. Lett.* **34**, 44 (1979); C. N. Man, A. Brillet, *Opt. Commun.* **45**, 95 (1983); W. Luhs, B. Wellegehausen, *Opt. Commun.* **46**, 121 (1983).

[25] Z. Drozdowicz, R. J. Temkin, R. Lax, *IEEE J. Quantum Electron.* **QE-15**, 170, 865 (1979); J. Heppner, C. O. Weiss, U. Hubner, G. Schinn, *IEEE J. Quantum Electron.* **QE-16**, 392 (1980).

[26] W. Gawlik, *Acta Phys. Pol.*, this issue.